



A method for an efficiency and weight-optimised preliminary design of a hydrogen-powered fuel cell-based hybrid-electric propulsion system for aviation purposes

Mücahit Akkaya¹ · Nicolai Neumann¹ · Dieter Peitsch¹

Received: 27 February 2023 / Revised: 13 September 2023 / Accepted: 7 November 2023 / Published online: 10 December 2023
© The Author(s) 2023

Abstract

There is a worldwide effort to advance the usage of zero-emission propulsion systems for aircraft. Due to their high thermodynamic efficiency and the fact that they produce no CO₂ and NO_x emissions, hydrogen-powered fuel cells are becoming increasingly popular for aviation purposes. However, fuel cell systems suffer from lower power density and higher cooling requirements when compared to conventional propulsion systems. Harnessing the high potential requires an optimised design of the whole propulsion system and its heat management system. This paper aims to present a method for the preliminary design and dimensioning of a fuel cell-based hybrid-electric propulsion system, which respects the limits of the heat management system and is weight and efficiency optimised. Thermodynamic models of the whole propulsion system are a crucial element to enable further investigations. Such a model has been developed, which is suitable for unsteady simulations of the propulsion and the heat management system performance of a short-range four-seater aircraft. A parameter study of the design parameters has been performed to display their impact on the system mass, the overall efficiency and the total hydrogen consumption. These results enable the identification of an overall optimised configuration. The study indicates that fuel cell-only configurations with an oversized fuel cell stack are beneficial for the analysed aircraft and flight mission.

Keywords Hybrid electric aircraft · PEM fuel cell · Preliminary design · Optimisation Performance

List of symbols

A	Area, m ²	γ	Flight path angle, °
α	Angle of attack, °	\dot{H}	Enthalpy change, W
ALT	Altitude m	h	Specific enthalpy, J/kg
C	Heat capacity rate, W/K	h	Heat transfer coefficient, W/(m ² K)
C	Battery capacity, J	H_u	Lower heating value, J/kg
c_D	Drag coefficient –	I	Current, A
c_L	Lift coefficient –	J	Advance ratio –
C_P	Power coefficient, –	κ	Ratio of specific heats –
c_p	Specific heat capacity, J/(kg K)	λ	Stoichiometric factor –
C_T	Thrust coefficient –	L	Lift force, N
D	Diameter, m	M	Mass, kg
D	Drag force, N	Δm_{H_2}	Hydrogen consumption, kg
E	Nernst voltage, V	M	Mach number of the aircraft –
ϵ	Effectiveness, –	\dot{m}	Mass flow, kg/s
η	Efficiency, %	\dot{m}_{red}	Reduced mass flow, ms \sqrt{K}
		N	Number of fuel cells in the stack –
		N	Shaft speed, 1/s
		NTU	Number of transfer units –
		P	Power W
		p	Pressure Pa
		Π	(Total) pressure ratio –
		q	Dynamic pressure, Pa

✉ Mücahit Akkaya
m.akkaya@tu-berlin.de

¹ Chair for Aero Engines, Institute of Aeronautics and Astronautics, Technische Universität Berlin, Marchstraße 12-14, 10587 Berlin, Germany

\dot{Q}	Heat flow, W
ρ	Density, kg/m ³
T	Temperature, K
t	Time, s
θ	Pitch angle, °
T	Thrust, N
TOM	Take-off mass, kg
U	Heat transfer coefficient, W/(m ² K)
v	Velocity m/s
\dot{v}	Rate of acceleration, m/s ³
W	Weight, N

Subscript

Air	Air
amb	Ambient
BAT	Battery
C	Compressor
ch	Chemical
col	Coolant
El	Electric
est	Estimated
f	Fluid
H/H ₂	Hydrogen
in	At component inlet
max	Maximum
min	Minimum
O/O ₂	Oxygen
out	At component outlet
Overall	Overall
Prop	Propulsive
ref	Reference
req	Required
s	Surface
Shaft	Shaft
stoich	Stoichiometric
Sys	System
util.	Utilised
W	Wing
x, z	Referring to coordinate axis

Abbreviations

ACARE	Advisory Council for Aeronautics Research and Innovation in Europe
ERDF	European Regional Development Fund
FC	Fuel cell (stack)
HEX	Heat exchanger
IBB	Business Development Bank of the Federal State of Berlin
PEM	Proton exchange membrane

1 Introduction

Sustainability is an important challenge that industries across all sectors must address in order to reduce their environmental footprint and thus their impact on the climate. The contribution of aviation to anthropogenic climate change is currently estimated at around 5% [1], which is trending upwards as air passenger traffic grows at a rate of 4% per year [2]. In the Flight Path 2050 document [3], the Advisory Council for Aeronautics Research and Innovation in Europe (ACARE) set a number of targets for reducing pollutant emissions. For example, CO₂ emissions are to be reduced by 75% per passenger-kilometre by 2050 compared to an aircraft in 2000. Research and development and the continuous replacement of older aircraft are leading to an increase in efficiency and thus a reduction in specific fuel consumption, resulting in lower pollutant emissions per passenger-kilometre. However, several recent projections indicate that efficiency improvements through further improvements in known technologies will not meet the goals of the Flight Path 2050 document [4, 5]. Therefore, it is necessary to explore the use of alternative, more radical approaches that will enable to meet the requirements.

The use of electric propulsion promises not only to provide energy conversion at a higher efficiency, but also to directly eliminate CO₂ and NO_x emissions during flight. One possibility is the use of batteries as a power source. Batteries have a major advantage due to their very high efficiency of 90% [6], as their losses are low and less waste heat is generated. However, batteries have a relatively low gravimetric energy and power density, which would result in a very high battery weight if used alone. In particular, the low energy density has a strong impact on the range, since range is directly correlated with available energy. Another challenge with batteries as the main power source is that they must either be replaced or recharged between flights, which would result in very long turnaround times given the current state of the art. An alternative electrical power source are fuel cells. Hydrogen-powered proton exchange membrane (PEM) fuel cells, for example, have a higher gravimetric power density than batteries, and their tanks can be filled with either cryogenic or pressurised hydrogen in a relatively short time between flights. Although fuel cells are relatively efficient compared to gas turbines or internal combustion engines, their efficiency is lower than batteries, resulting in higher losses and thus more waste heat. Since fuel cells do not have a high exhaust mass flow, as i.e. gas turbines, the heat generated must be removed by a heat management system.

Hybridisation approaches that combine batteries and fuel cells can create synergy effects. For example, one

advantage is that batteries support the fuel cell stack in high-performance phases, resulting in a lower required maximum power of the fuel cell stack. Kadyk et al. [7] conducted a design study of a hybrid propulsion unit for an Airbus A320. They demonstrate that hybridisation benefits depend on mission range. For a mid-range application hybrid designs with a reduced fuel cell size yield a reduced fuel consumption.

Alternatively, the fuel cell system could be kept constant and would hence be oversized. Oversizing the fuel cell system could be a valuable design strategy. There are at least two strategies to benefit from an oversized fuel cell system as proposed and described in the work of Kasim et al. [8]. Assuming a power requirement of 150 kW provided by four 50 kW stacks. The fuel cell stacks could be operated in a daisy-chained mode. That means that during each flight, one of the four fuel cell stacks is rotationally deactivated, which preserves the lifetime of all four fuel cell stacks and eliminates degradation without having to change the fuel cell stacks between two flights. Alternatively, in order to achieve the required power, the power output of each stack could be reduced. In that case, the stacks are operated at part load, which leads to a higher efficiency. Kasim et al. [8] estimate a fuel burn reduction by 10% for a typical Cessna 208 Caravan and a 350 km flight mission.

Kadyk et al. [9] also stress that the fuel cell stack needs to be designed in the context of the whole energy system. They suggest that the fuel cell stack should always be at least slightly oversized to avoid the efficiency penalty close to maximum fuel cell stack power. Moreover, depending on the application, further oversizing, i.e. investing in a larger and heavier fuel cell stack in order to gain a more efficient process, might be beneficial. They provide a performance cost-benefit curve for a propulsion system for an Airbus A320. According to them, the ratio of energy-to-power determines the optimal oversize of the stack.

In [9], however, the aircraft was powered only by fuel cells. The combination of fuel cells and a battery greatly expands the design space. For example, the use of a stronger battery increases the weight of the battery and thus the system weight. On the other hand, a stronger battery leads to a lower required maximum power of the fuel cell stack, so that either the fuel cell stack can be shrunk, reducing the weight of the fuel cell stack, or the fuel cell stack can remain at constant dimensions but operated at a lower power, increasing its efficiency. The consideration of both effects is of great importance to find an efficiency and weight-optimised propulsion system design for an aircraft.

This paper presents a model based method for the efficiency and weight-optimised sizing of a hydrogen-powered fuel cell-based hybrid-electric aircraft respecting the limits of a set heat management system. The process of this design method is shown as flowchart in Fig. 1. For this purpose, a

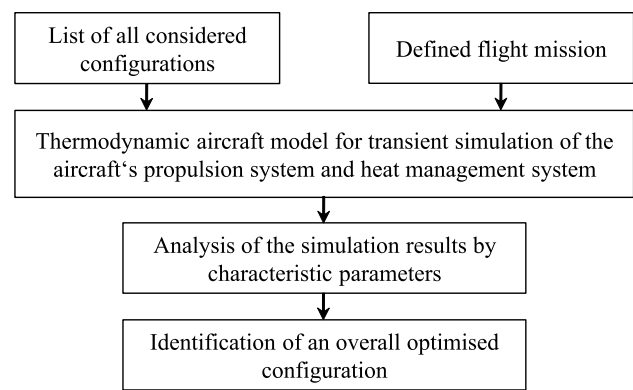


Fig. 1 Flowchart of the preliminary design methodology

model of a four-seater hybrid-electric aircraft was created. This model is then used to simulate the transient behaviour of the propulsion system and its heat management system during a typical flight mission. The simulations are conducted for a number of different fuel cell stack and battery configurations. Key parameters such as maximum stack temperature, overall efficiency, total hydrogen consumption, and system mass of the fuel cell stack and battery are compared. A “sweet spot area” where an optimised overall design would be possible is identified.

The field of fuel cell-based hybrid-electric aircraft propulsion systems is relatively new and thus there is a lack of published data that can be utilised for the design. Hence, to be able to build a model for the proposed design method, besides published data, assumptions have to be made based on industrial and academic experience. For that, an aircraft manufacturer that researches hybrid-electric aircraft was consulted. However, as this paper mainly describes the method itself, as well as having preliminary design character, the proposed assumptions can be replaced if more accurate assumptions can be made or more detailed data is available.

2 Methods and models

This section covers the models and methods of this paper. First, the aircraft, its propulsion system and its heat management system will be described. Subsequently, the models for the preliminary design methodology are introduced.

2.1 Concept aircraft

A preliminary design method of the propulsion system for a hybrid-electric short-range four-seater aircraft shall be presented. It is assumed that the take-off mass, excluding the battery and the fuel cell stack, remains at 2000 kg independent from the actual power battery and fuel cell stack masses.

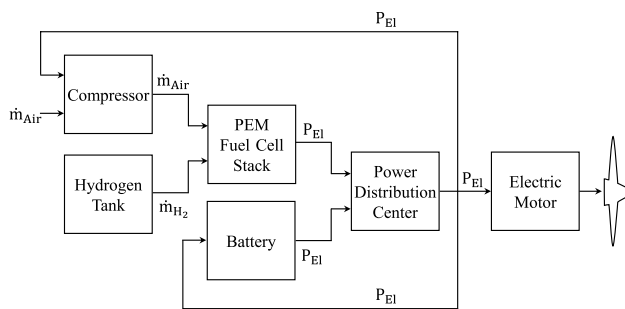


Fig. 2 Flowchart of the aircraft's propulsion system (one side)

Thus, the impact of mass changes of individual components on the aircraft's structure is neglected. Furthermore, the wing area A_W is estimated at 18 m^2 . The assumptions of the aircraft's take-off mass as well as its wing area are in line with aircraft of the same aircraft class [10–12]. Exemplary diagrams for the lift and drag polars were used, provided by an aircraft manufacturer.

2.2 Propulsion system

The architecture of the aircraft's propulsion system is depicted in Fig. 2 for one side of the aircraft, as the propulsion system is completely symmetric. The required thrust is generated by one propeller on each side of the aircraft, which is driven by an electric motor. The electric motor is supplied with electric power from the fuel cell stack during lower power levels, or by the fuel cell stack and the battery during higher power levels. Additionally, as the battery discharges during high power levels, it is charged during lower power levels such as cruise. The propulsion system also requires a compressor, as the fuel cell stack is operated at a higher pressure than ambient pressure. Hence, a part of the generated electric power is supplied to the compressor. The power demand of secondary subsystems, i.e. coolant pumps or aircraft electronics has been neglected, as their power demand is very small relative to the primary components of the propulsion system.

2.3 Heat management system

The heat management is one of the most crucial aspects regarding the utilisation of fuel cells, therefore a proper heat management system must be designed [13]. In this paper, the fuel cell stack is actively cooled with a heat exchanger (FC-HEX), using a liquid coolant, as demonstrated schematically in Fig. 3 for one side of the aircraft. After cooling the fuel cell stack, coolant is pumped into a second heat exchanger, in which it is cooled by air. The air intake is integrated into the nacelle downstream of the propeller increasing the heat exchanger's driving pressure difference. The coolant is then

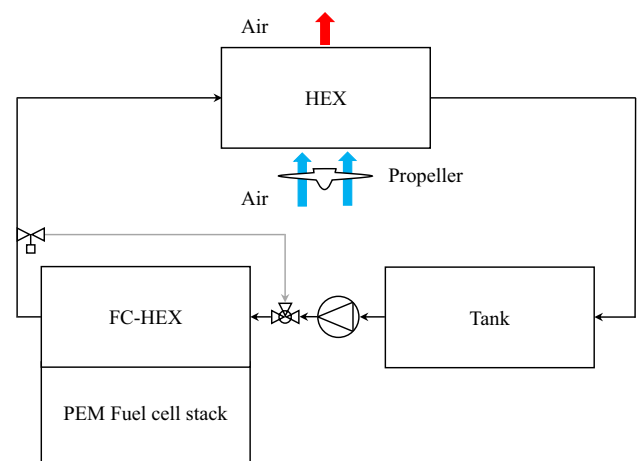


Fig. 3 Flowchart of the aircraft's heat management system (one side)

returned into the coolant tank, which supplies the coolant fluid for the whole heat management cycle. As the fuel cell stack also has a minimum temperature limit, a valve downstream of the FC-HEX allows to recirculate a portion of the coolant. Thus, the coolant temperature at the entrance of the FC-HEX increases, facilitating a faster warm up.

Although, other components such as the battery or the electric motor also generate heat and must therefore be cooled, they will not be further discussed within this paper. The cooling requirement of the electric motor is relatively independent of the investigated design parameters, as it mainly depends on the motor efficiency. The battery however, is only used for a relatively short time and operates with a very high efficiency. Therefore, relatively low waste heat is generated for a relatively short time. It is therefore decided, that the battery cooling is not within the scope of this work, as the focus is on the fuel cell stack cooling. However, for future investigations, the heat management model can be extended to also consider the cooling of further components, i.e. the battery and the electric motor.

2.4 Models

The presented design method is based on an aircraft model that simulates the transient behaviour of the aircraft's propulsion system and heat management system. The general structure of the aircraft model for the preliminary design method is represented in Fig. 4.

As shown, the model is split into four interacting sections. The first section, called atmosphere model, determines the atmospheric properties during flight. As the temperature and pressure change with altitude, the atmospheric properties must be determined at each time step. The second section is the thrust demand model, which determines the thrust demand at each time step. The

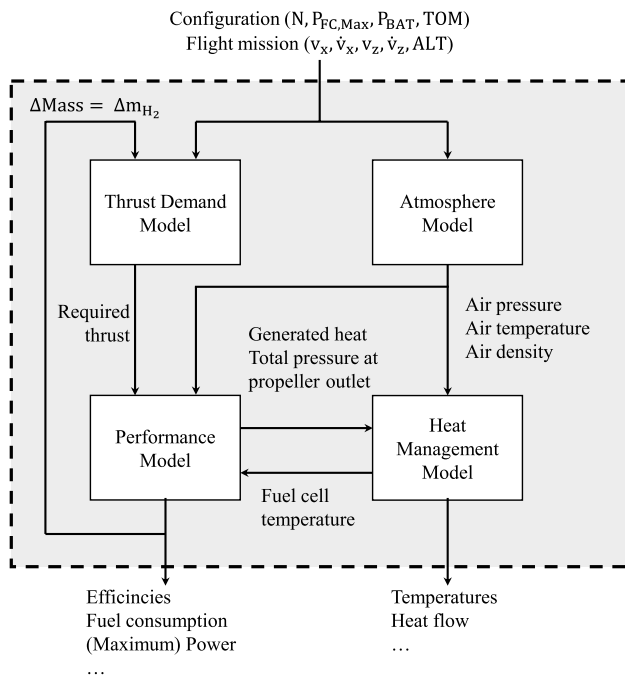


Fig. 4 Flowchart of the aircraft model

required thrust is computed for a constant flight mission taking into account the aircraft weight, which in turn depends on the sizes of the battery and the fuel cell stack. The ambient air properties and the required thrust are inputs into the two main sections: the performance model which simulates the behaviour of all primary components of the propulsion system and the heat management model which simulates the behaviour of the heat management system. On one hand, the heat management model requires the generated heat, which results from the performance model as it is able to determine the occurring losses. Furthermore, the heat management model requires inputs describing the propeller behaviour, as the air intake for the air heat exchanger sits downstream of the propeller. On the other hand, the performance of the fuel cell stack depends on its temperature which is computed in the heat management model. Therefore, the performance model and the heat management model are in a continuous exchange of information. The performance model also determines the consumed hydrogen, which defines the change in mass during flight.

Due to these interactions, the aircraft model is of a highly iterative nature. Furthermore, due to transient operation phases and due to its dynamic characteristics, the model consists of a vast number of mathematical equations containing several differentials. Therefore, Matlab/Simulink is used to set up and combine the models into the overall aircraft model, as shown in Fig. 4.

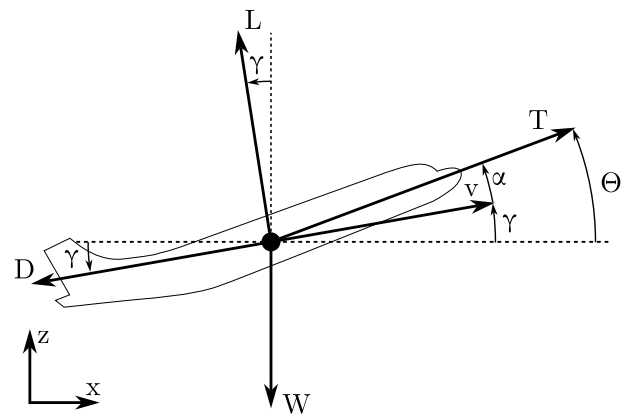


Fig. 5 Coordinate system for the force equations

2.4.1 Thrust demand model

The flight mission defines the acceleration as well as all velocity components of the aircraft. Furthermore, the altitude of the aircraft is set within the flight mission. This model determines the thrust demand to satisfy the requirements set by the flight mission. For that, the mass of the aircraft is used as an input at each time step of the flight mission.

To determine the required thrust, the aircraft dynamics and therefore all forces that act on the aircraft during flight must be considered. All assumptions, as well as approximations and definitions regarding aircraft dynamics are based on Hull [14] and Yechout et al. [15]. The aircraft is viewed as a point-mass, in which all forces are applied to the aircraft's center of gravity. Furthermore, the earth is approximated as a flat, non-rotating, inertial reference frame. It is also assumed that the atmosphere does not move relative to the earth. Additionally, only longitudinal and vertical movements are considered, neglecting any lateral movement. Therefore, the position of the aircraft is defined by its x and z coordinates, as well as its pitch angle θ, which describes the deviation of the aircraft's axis to its reference coordinate system. A second angle that can be defined is the flight path angle γ, which describes the movement of the aircraft within the coordinate system, defined in Eq. (1). A windless operation is assumed, therefore, the angle of attack α is defined as the deviation between the flight path angle and the pitch angle.

$$\tan(\gamma) = \frac{dz}{dx} = \frac{\dot{z}}{\dot{x}} = \frac{v_z}{v_x} \tag{1}$$

During flight, the main forces are the weight W, the thrust T, the drag D and the lift L as shown in Fig. 5. The drag force acts tangentially to the flight path angle, whilst the lift

applies vertically. Assuming, that the propeller and the aircraft are aligned, the thrust is always tangential to the pitch angle. The weight always applies directly towards the negative z-axis of the reference system. The force equation can be defined for each axis, which results in the Eqs. (2) and (3).

$$M \cdot \dot{v}_x = T \cdot \cos(\theta) - L \cdot \sin(\gamma) - D \cdot \cos(\gamma) \quad (2)$$

$$M \cdot \dot{v}_z = T \cdot \sin(\theta) + L \cdot \cos(\gamma) - D \cdot \sin(\gamma) - W \quad (3)$$

The aircraft velocity v , as well as the accelerations \dot{v}_x and \dot{v}_z are predefined by the flight mission. The mass is defined by the configuration and the consumed hydrogen. The lift coefficient c_L can be determined for the angle of attack α by the aircraft's lift polar, whilst the drag coefficient c_D can be determined by using the aircraft's drag polar. As the angle of attack directly correlates with the pitch angle, the only two independent variables in this system of two equations (Eqs. 2, 3) are the pitch angle and the thrust. Therefore, the system of equations can be solved iteratively to determine the thrust demand.

2.4.2 Performance model

The propulsion system, as shown in Fig. 2, consists of several main components, which need to be modelled individually. The modelling of the main components such as the fuel cell stack, the battery, the compressor, the electric motor and the propeller will be presented in this section.

PROPELLER The propeller model uses a propeller map, which delivers the thrust coefficient C_T for a combination of advance ratio J and power coefficient C_P (see Eqs. 4, 5) [16, 17]. The advance ratio and the power coefficient can be determined by the shaft speed N , the propeller diameter D , the aircraft velocity v and the shaft power P_{Shaft} , which are all inputs of the propeller model.

$$J = \frac{v}{D \cdot N} \quad (4)$$

$$C_P = \frac{P_{\text{Shaft}}}{\rho \cdot N^3 \cdot D^5} \quad (5)$$

The advance ratio and the power coefficient are then used to interpolate the thrust coefficient by the propeller map, which enables to determinate the generated thrust T by Eq. (6) [16, 17]. A PID-Controller is used to vary the shaft power, until the thrust of the propeller model matches the required thrust of the thrust demand model.

$$T = C_T \cdot \frac{\rho}{2} \cdot N^2 \cdot D^4 \quad (6)$$

The thrust can then be used to determine the outlet velocity of the propeller v_{out} by Eq. (7) [16], which enables to

compute the dynamic pressure at the outlet of the propeller q_{out} by Eq. (8). It is assumed, that the dynamic pressure can be utilised as the available pressure difference Δp for the air flow in the air heat exchanger, which sits downstream of the propeller.

$$v_{\text{out}} = \sqrt{\frac{T \cdot 8}{\rho \cdot \pi \cdot D^2} + v^2} \quad (7)$$

$$q_{\text{out}} = \frac{\rho}{2} v_{\text{out}}^2 \quad (8)$$

Electric motor Electric motors are well known to operate at a relatively constant efficiency over a broad operating envelope. Hence, in this model, the electric motor efficiency η_{EM} is set constant at 95% [6], which is a conservative approach, as modern electric motors operate at even higher efficiencies. The generated shaft power P_{Shaft} of the electric motor can therefore be determined by Eq. (9) based on the supplied electric power P_{El} .

$$P_{\text{Shaft}} = \eta_{\text{EM}} \cdot P_{\text{El}} \quad (9)$$

Battery Batteries are mostly described by two parameters, the total capacity and the maximal electric power. Analogue to the electric motor, the battery efficiency is assumed to be constant, as batteries also operate at relatively constant efficiencies. The battery efficiency η_{BAT} is assumed to be 90% [6] during both discharging and charging. During battery charging, the supplied electric power P_{El} is converted into chemical power P_{ch} as in Eq. (10). During discharge, the chemical power is converted into electric power as in Eq. (11).

$$P_{\text{ch}} = \eta_{\text{BAT}} \cdot P_{\text{El}} \quad (10)$$

$$P_{\text{ch}} = \frac{P_{\text{El}}}{\eta_{\text{BAT}}} \quad (11)$$

The change in the capacity ΔC over a period of time Δt can therefore be determined by Eq. (12).

$$\Delta C = \int_t^{t+\Delta t} P_{\text{ch}} dt \quad (12)$$

Fuel cell stack As the fuel cell stack is the main power source, its behaviour is modelled in more detail. The thermodynamic maximum output voltage E , that a single fuel cell can deliver, can be determined in volts by the Nernst equation, which is shown in Eq. (13) [18–20], consisting of the fuel cell temperature T_{FC} , and the partial pressures of hydrogen P_{H_2} and oxygen P_{O_2} .

$$E = 1.229 - 0.85 \cdot 10^{-3} \cdot (T_{FC} - 298.15) + 4.3085 \cdot 10^{-5} \cdot T_{FC} \cdot \left[\ln(P_{H_2}) + \frac{1}{2} \cdot \ln(P_{O_2}) \right] \quad (13)$$

The real cell voltage V is implemented by a polarisation curve, which depicts the cell voltage as a function of current. The polarisation curve [21] describes the cell behaviour for a defined cell temperature and pressure. The compressor enables the fuel cell to be operated at exactly that pressure for which the polarisation curve is displayed. The impact of a temperature variation on the operation behaviour is not implemented. However, the heat management system aims to operate the fuel cell stack at a relatively narrow temperature range.

The power that is generated can therefore be determined for a single cell by multiplying the cell voltage V and the current I . In order to determine the total electric power of the fuel cell stack P_{Stack} , the power of a single cell must be factorised by the number of cells of the fuel cell stack N , resulting in Eq. (14).

$$P_{Stack} = N \cdot V \cdot I \quad (14)$$

The difference between ideal and real fuel cell performance is due to losses, which are removed in terms of heat. Hence, the heat for a single cell is determined by the difference between the Nernst voltage E and the cell real voltage V multiplied by the current I . This result is then multiplied by the number of fuel cells in the stack to determine the total heat generated in the fuel cell stack \dot{Q}_{Stack} , as shown in Eq. (15) [13].

$$\dot{Q}_{Stack} = N \cdot (E - V) \cdot I \quad (15)$$

In order to determine the total hydrogen consumption, the rate of hydrogen reacting in the fuel cell stack needs to be obtained. For that, the current can be divided by the Faraday constant F , which results in the flow rate of electrons per fuel cell. In order to get the flow rate of electrons of the whole stack \dot{N}_{e^-} , this must be multiplied by the number of fuel cells in the stack. Each reacting hydrogen atom supplies one electron. Therefore, the flow rate of electrons equals the reaction rate of hydrogen atoms \dot{N}_H . This can be used to determine the mass flow rate of hydrogen \dot{m}_{H_2} , that is used for the reaction, by multiplying the molar mass of hydrogen M_H , as demonstrated in Eq. (17) [22]. Assuming that no hydrogen diffuses without being involved in the reaction, the hydrogen consumption rate equals the mass flow rate of the reacting hydrogen. By integrating this mass flow rate over the whole flight, the total hydrogen consumption Δm_{H_2} can be determined, as shown in Eq. (18).

$$\dot{N}_H = \dot{N}_{e^-} = \frac{N \cdot I}{F} \quad (16)$$

$$\dot{m}_{H_2} = \dot{N}_H \cdot M_H = \frac{N \cdot I \cdot M_H}{F} \quad (17)$$

$$\Delta m_{H_2} = \int_{t_{start}}^{t_{end}} \frac{N \cdot I \cdot M_H}{F} dt \quad (18)$$

Analogue to that, the required air flow can be determined. Two hydrogen atoms react with one oxygen atom. Therefore, the reaction rate of oxygen atoms equals half of the reaction rate of hydrogen atoms. This rate can then be multiplied with the molar mass of oxygen M_O , in order to determine the mass flow rate of oxygen that reacts in the fuel cell stack \dot{m}_{O_2} . For dry air, oxygen only makes up 23.01% [23] of the mass, thus the air flow that would be needed for a stoichiometric reaction $\dot{m}_{air,stoich}$ can be determined by Eq. (20). However, this air flow would only satisfy if every oxygen atom also reacts. As this is not to be assumed, surplus of air needs to be supplied to satisfy the needs of the fuel cell stack. In the literature, varying stoichiometric factors λ can be found, which is assumed as 2 [20] for this paper. Hence, the compressor needs to supply an air flow which is determined by Eq. (21) [22].

$$\dot{m}_{O_2} = \frac{\dot{N}_H}{2} \cdot M_O = \frac{N \cdot I \cdot M_O}{F \cdot 2} \quad (19)$$

$$\dot{m}_{air,stoich} = \frac{\dot{m}_{O_2}}{0.2301} = \frac{N \cdot I \cdot M_O}{F \cdot 2 \cdot 0.2301} \quad (20)$$

$$\dot{m}_{air} = \lambda \cdot \dot{m}_{air,stoich} = \frac{N \cdot I \cdot M_O \cdot \lambda}{F \cdot 2 \cdot 0.2301} \quad (21)$$

Compressor The compressor provides air to the fuel cell stack at its required pressure. In this case, the air is compressed to a pressure of 2 bar. The required power for the compressor P_C can be determined by Eq. (22), in which η_C is the isentropic compressor efficiency, c_p is the specific heat capacity of air, Π is the total pressure ratio of the compressor, and κ is the ratio of specific heats.

$$P_C = \frac{1}{\eta_C} \cdot c_p \cdot \dot{m}_{air} \cdot \left(\Pi^{\frac{\kappa-1}{\kappa}} - 1 \right) \quad (22)$$

The total pressure ratio of the compressor is defined as the ratio between the total pressure at the outlet of the compressor to the total pressure at its inlet. When the outlet velocity of the compressor is neglected, assuming that the air passes through the fuel cell slowly to enable a reaction, the total pressure at the outlet can be set to the required operating pressure of 2 bar. Assuming a total pressure loss of 2% within the air intake, the total pressure at the inlet of the compressor can be determined by the total pressure at the inlet of the air intake. Hence, the required total pressure ratio

is determined by Eq. (23), in which p_{amb} is the ambient static pressure and M is the Mach number describing the aircraft velocity.

$$\Pi = \frac{2 \text{ bar}}{0.98 \cdot \left[p_{amb} \cdot \left(1 + \frac{\kappa-1}{2} M^2 \right)^{\frac{\kappa}{\kappa-1}} \right]} \quad (23)$$

2.4.3 Heat management model

The heat management system is depicted in Fig. 3. The models of the fuel cell stack, the fuel cell stack heat exchanger, the air heat exchanger and the tank are introduced next.

Fuel cell stack The fuel cell stack is modelled as a thermal mass, which is characterised by its specific heat capacity c_p , its mass M_{FC} and its temperature T_{FC} . To determine the temperature of the fuel cell stack during the flight, the energy balance considering all heat flows must be used. As mentioned earlier, heat is generated within the fuel cell stack, which is represented by \dot{Q}_{Stack} . Furthermore, heat is removed by the fuel cell heat exchanger denoted \dot{Q}_{FC-HEX} . Other heat transfer mechanisms such as radiation and heat transfer to surrounding air have been neglected. Also, energy associated with incoming and outgoing fluids has been ignored. Thus, the energy balance can be written as shown in Eq. (24) [13, 22]:

$$c_p \cdot M_{FC} \cdot \frac{dT_{FC}}{dt} = \Sigma \dot{H} = \dot{Q}_{Stack} - \dot{Q}_{FC-HEX} \quad (24)$$

Hence, to determine the temperature at each time step, the temperature gradient $\frac{dT_{FC}}{dt}$ must be determined. Therefore, the heat which dissipates through the fuel cell stack heat exchanger \dot{Q}_{FC-HEX} is required.

Fuel cell stack heat exchanger The fuel cell stack heat exchanger is modelled as a solid wall along which coolant is passed. A general approach to describe the forced convective heat flow between a surface and a fluid is shown in Eq. (25), in which h is the heat transfer coefficient, A_{Heat} is the heat transfer area, T_s is the temperature of the surface area whilst T_f describes the temperature of the fluid [22, 24].

$$\dot{Q} = h \cdot A_{Heat} \cdot (T_s - T_f) \quad (25)$$

One main factor of the heat flow is the temperature difference, which is not constant over the whole heat transfer area, hence Eq. (25) cannot be applied directly. Therefore, adjustments have to take place in order to determine the heat flow within the heat exchanger. It is assumed, that the heat transfer coefficient is constant over the whole heat exchanger. Furthermore, it is assumed that the surface temperature, describing the fuel cell stack, is homogeneous whilst the coolant temperature changes between the entrance and outlet

of the heat exchanger. The total heat transfer area A_{heat} is split into infinitesimal small sections in which the coolant temperature is assumed constant. Therefore, the Eq. (25) can be applied for each section individually. However, the fluid temperature of a section is determined by the heat flow and the fluid temperature in the previous section. This method leads to a differential equation, which when solved results in Eq. (26). This equation can also be derived by utilising the definition of the log mean temperature difference, as the same approach is applied [25]. The Eq. (26) enables to determine the coolant temperature at the FC-HEX outlet $T_{col,out}$ with the fuel cell stack temperature T_{FC} , the coolant flow \dot{m}_{col} , the specific heat capacity of the coolant c_p and the coolant temperature at the FC-HEX inlet $T_{col,in}$. The total heat flow in the FC-HEX \dot{Q}_{FC-HEX} can hence be determined by Eq. (27).

$$T_{col,out} = T_{FC} - (T_{FC} - T_{col,in}) \cdot e^{-\frac{h \cdot A_{Heat}}{\dot{m}_{col} \cdot c_p}} \quad (26)$$

$$\dot{Q}_{FC-HEX} = c_p \cdot \dot{m}_{col} \cdot (T_{col,out} - T_{col,in}) \quad (27)$$

Air heat exchanger The heat is removed from the heat management system by the air heat exchanger. The heat exchanger is modelled as a cross heat exchanger. Data for individual operating points was provided by the manufacturer, in order to describe the behaviour of the heat exchanger correctly. The data points are used to derive characteristic curves, which were cast into a model.

The air heat exchanger is modelled with the ϵ -NTU method. First, the air mass flow must be determined. For that, the characteristic curve in Fig. 6 is used, which describes the reduced air mass flow of the heat exchanger \dot{m}_{red} as a function with respect to the available pressure ratio Π . The values in Fig. 6 are normalised by referring

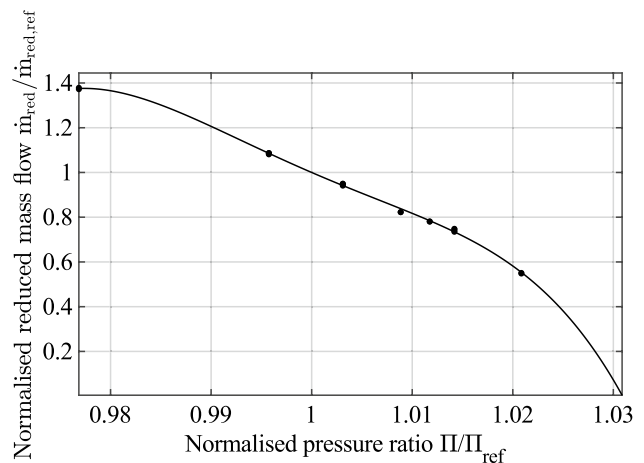


Fig. 6 Characteristic curve describing the reduced air mass flow \dot{m}_{red} with respect to the available pressure ratio Π

each absolute value to predefined reference values $\dot{m}_{red,ref}$ and Π_{ref} .

The available pressure ratio is defined as shown in Eq. (28) by the ambient pressure p and the available pressure difference Δp at the propeller outlet. However, the reduced air mass flow of the heat exchanger is defined by the absolute air mass flow \dot{m}_{air} , the ambient pressure p and the air temperature at outlet of the heat exchanger $T_{air,out}$. To initiate the iteration, a proper outlet air temperature is guessed to determine the air mass flow.

$$\Pi = \frac{p}{p + \Delta p} \tag{28}$$

$$\dot{m}_{red} = \frac{\dot{m}_{air} \cdot \sqrt{T_{air,out}}}{p + \Delta p} \tag{29}$$

Once the air flow is determined, the heat capacity rate C can be calculated for the coolant flow and the air flow, as product of the mass flow \dot{m} and the specific heat capacity c_p . The lower value defines the minimum heat capacity rate C_{Min} and the higher value defines the maximum heat capacity rate C_{Max} . The air flow and the coolant flow are used for the heat exchanger map in Fig. 7, which is derived from a set of characteristic curves. Each curve describes the product of the heat transfer coefficient U and the heat transfer area A over the air flow for a specific coolant flow. A linear interpolation is applied for deviating coolant flows. To normalise the values in the heat exchanger map in Fig. 7, each value is divided by its corresponding reference value.

The product $U \cdot A$ can then be used to determine the unitless characteristic value NTU, as shown in Eq. (30) [24, 26]. Additionally, the second characteristic value, generally referred as the heat capacity ratio C_r , can be determined by Eq. (31) [24, 26].

$$NTU = \frac{U \cdot A}{C_{Min}} \tag{30}$$

$$C_r = \frac{C_{Min}}{C_{Max}} \tag{31}$$

These two characteristic values can be applied to the correlation in Eq. (32), which gives the effectiveness ϵ . The minimum heat capacity rate and the inlet temperature of the air and the coolant are used to determine the maximum heat flow \dot{Q}_{Max} as shown in Eq. (33) [24].

$$\epsilon = 1 - e^{-C_r^{-1} \cdot NTU^{0.22} \cdot (e^{-C_r \cdot NTU^{0.78}} - 1)} \tag{32}$$

$$\dot{Q}_{Max} = C_{Min} \cdot (T_{col,in} - T_{air,in}) \tag{33}$$

Once the effectiveness and the maximum heat flow are determined, they can be used to calculate the real heat flow \dot{Q}_{HEX} , as shown in Eq. (34). As the calculation is done based on an estimation for the air outlet temperature $T_{air,out}$, the determined heat flow can be used to calculate a new outlet temperature, which starts the next iteration step, until the temperature converges.

$$\dot{Q}_{HEX} = \epsilon \cdot \dot{Q}_{Max} \tag{34}$$

Tank The coolant within the tank is modelled as a homogeneous thermal mass, with the specific heat capacity of the coolant c_p , the total tank capacity M , and the temperature of the coolant within the tank T_{Tank} . Analogous to the fuel cell stack, the energy balance is needed to determine the coolant temperature. Therefore, the enthalpy of the incoming and outgoing coolant must be considered. For the tank, it is approximated that at each time step no mass is accumulated. Hence, incoming and outgoing mass flow are identical. Additionally, it is assumed that the temperature of the outgoing coolant flow equals the temperature of the coolant within the tank. Therefore, the resulting energy balance is shown in Eq. (35).

$$c_p \cdot M \cdot \frac{dT_{Tank}}{dt} = \dot{m}_{col} \cdot c_p \cdot (T_{in} - T_{Tank}) \tag{35}$$

2.5 Model validation suggestions

The validation of a model, that simulates the operational behaviour of a multi-component system and thus the interaction of different components is equally challenging as it is important for its reliability. In order to have a representative model however, the most relevant components are modelled based on the physical characterisation of the component's behaviour. Hence, it is assumed that the model accuracy is sufficient and will thus be used for the proposed method in

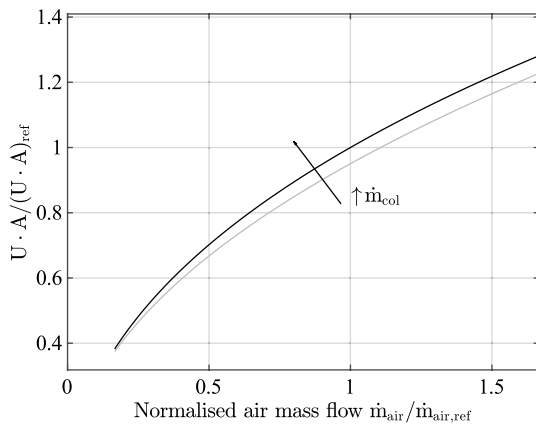


Fig. 7 Heat exchanger map

this paper, as the validation is out of the scope of this work. However, suggestions regarding validation will be provided for further investigations.

To validate the model for a certain configuration, all components are needed. These components need to be utilised for individual tests on component level, to derive the component characteristics, which need to be implemented into the model. For these tests, it is important to investigate the component behaviour in its entire operational range. Additionally, besides steady-state tests, for some components, it might be beneficial to add transient tests, to be able to describe the component's dynamic behaviour, i.e. limits for acceleration and deceleration or its thermal inertia.

After providing the model with all derived characteristics, either the whole system, or a subgroup of interacting components can be built into a test-bed which needs sufficient instrumentation. A test with a defined power curve shall be performed on the test-bed and a simulation is to be performed with the model at the same power settings and the same ambient condition as in the test. Characteristic parameters such as temperatures, pressures and electrical as well as mechanical power, which are measured in the test-bed, shall be compared to the simulation results. If the difference between simulation and test is significant for certain parameters, the data must be used to derive physical explanations for this error, which can then be quantified and implemented into the model. Once there are no significant errors, the model can be considered validated.

3 Parameter study

The presented model simulates the behaviour of the propulsion system and the heat management system over a defined flight mission for different fuel cell stack and battery sizes. This section gives insights of the performed parameter studies.

3.1 Flight mission

A flight mission is defined with a cruise phase at an altitude of 8000 ft, a cruise velocity of 58.9 m/s and a cruise duration of 3 h. That yields a total mission range of 700 km.

Figure 8 shows the flight mission schematically with its altitude over time, as well as the required electric power $P_{El,req}$ for the propulsion system and the electric power which is supplied by the fuel cell stack P_{FC} . The deviation of the required electric power and the supplied electric power by the fuel cell stack defines the battery power. When the required power is larger than the supplied electric power of the fuel cell stack, the battery is discharged. When the supplied power of the fuel cell stack is larger i.e. during cruise, the surplus of power is utilised to charge the battery. Once

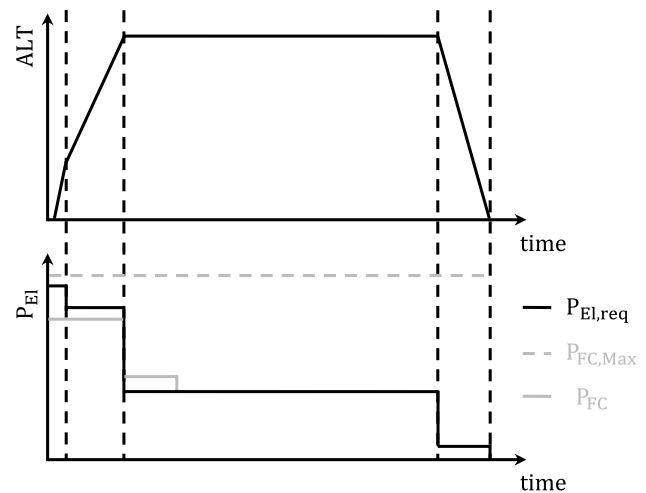


Fig. 8 Power distribution during the flight mission

the battery is fully charged, the fuel cell stack load reduces to match the required power of the propulsion system. As the fuel cell stack can be oversized, the maximum available power of the fuel cell stack $P_{FC,Max}$ does not have to match its maximum utilised power.

3.2 Parameter variation

The parameter study varies the fuel cell stack and the battery. The dimension of each individual fuel cell of the stack is assumed to remain constant. Therefore, only the number of cells N within the stack is varied. An increasing number of cells within the stack leads to an increasing maximum power of the fuel cell stack. The P-Stack of the manufacturer PowerCell is used as a reference. The datasheet [21] delivers a polarisation curve, describing the cell behaviour. Furthermore, the maximum power, weight and geometry data are available for several configurations with different fuel cell counts in the stack. This data is used to derive a linear correlation that describes the maximum power of the fuel cell stack in kilowatts as a function with respect to the number of fuel cells N , as shown in Eq. (36).

$$P_{FC,Max} = 0.2772 \cdot N - 1.0815 \quad (36)$$

Furthermore, the data suggests that the fuel cell stack mass does not increase exactly linearly with power. Therefore, the two largest configurations are used as a reference, in order to derive the correlation in Eq. (37) for the approximated fuel cell stack mass M_{FC} in kilogrammes with respect to the number of fuel cells. These two configurations are within the range required for this study.

$$M_{FC} = 0.0556 \cdot N + 16.722 \quad (37)$$

Changes in fuel cell count are also considered in the fuel cell stack heat exchanger model. It is assumed, that the heat transfer coefficient h is constant, whilst the heat transfer area A_{Heat} increases linearly with the number of fuel cells N . By utilising an estimated value for one case, provided by an aircraft manufacturer, the linear correlation in Eq. (38) was derived, which describes the product $h \cdot A_{\text{Heat}}$ in kilowatts per kelvin with respect to the number of fuel cells.

$$h \cdot A_{\text{Heat}} = 0.02 \cdot N \quad (38)$$

By these approximations, all relevant characteristic parameters within the model are a function of the number of fuel cells within the stack. Hence, the first parameter of the study is the number of fuel cells N . The second component that needs to be defined is the battery. In general, to approximate the battery mass, the energy density or the power density is utilised. For that, the battery mass is determined by the required power and the power density and by the required energy and the energy density. Whatever is more demanding defines the mass of the required battery. For this paper, the energy density of batteries is assumed to be 0.8 kWh/kg [7], whereas a power density of 0.5 kWh/kg is assumed. However, neither the maximum required battery power, nor the required total energy of the battery is defined before the simulation is performed. Therefore, the battery power or energy is not used as second parameter for the parameter study. Rather, the maximum utilised power of the fuel cell stack is used as the second parameter of this study. Based on this power, a maximum power of the battery is estimated. Initial simulations with the model presented in Sect. 2.4 show, that the required peak power is about 170 kW per side of the aircraft. Hence, for the initial run, the battery mass is determined by the estimated maximum power of the battery $P_{\text{BAT,est}}$, which is determined in kilowatts by Eq. (39). This power is then used to determine the estimated battery mass $M_{\text{BAT,est}}$ in kilogrammes by utilising the power density as shown in Eq. (40).

$$P_{\text{BAT,est}} = 170 - P_{\text{FC,max,util.}} \quad (39)$$

$$M_{\text{BAT,est}} = \frac{P_{\text{BAT,est}}}{0.5} \quad (40)$$

The fuel cell stack mass as well as the battery mass are then used to determine the maximum take-off mass, which is utilised to set the configuration for the model. Hence, the simulation can now be performed. The results of the simulation deliver a maximum required battery power P_{BAT} and a required total energy C_{BAT} of the battery. This is then utilised to determine the battery mass in kilogrammes as shown in Eq. (41). This iteration is performed several times, until the battery mass stabilised, hence the estimated battery

mass before the simulation equals the battery mass after the simulation.

$$M_{\text{BAT}} = \max\left(\left[\frac{P_{\text{BAT}}}{0.5}, \frac{C_{\text{BAT}}}{0.8}\right]\right) \quad (41)$$

Hence, the size of the battery can be changed by the variation of the maximum utilised power of the fuel cell stack. It is therefore sufficient for the battery and the fuel cell stack to vary the number of fuel cells N and the maximum utilised power of the fuel cell stack $P_{\text{FC,Max,util.}}$. For this study, the number of fuel cells within the stack is varied between 400 and 800 in increments of 50, whereas the maximum utilised electric power of the fuel cell stack is varied between 75 kW and 180 kW in increments of 15 kW, leading to a total of 72 different configurations.

4 Results

The results of the performed parameter study will be analysed in this section. To ease the evaluation of the results, all configurations are compared to a reference configuration. A common approach for hybridisation would be to size the fuel cell stack based on the required power in the climb phase. Therefore, the battery is only required to aid the fuel cell stack during the take-off phase. Furthermore, the available power of this configuration still enables the fuel cell stack to charge the battery during the cruise phase. Initial calculations show, that the climb phase requires approximately up to 120 kW electric power for the propulsion system. Therefore, for the reference configuration, the maximum utilised power of the fuel cell stack is kept at 120 kW. However, prior to this paper, the literature shows that oversizing might be beneficial regarding efficiency whilst the mass increases. Therefore, for the reference configuration, the fuel cell stack will be slightly oversized with a maximum available power of 130 kW to increase the efficiency without increasing the mass significantly. As the initial calculations also showed a peak power demand of approximately 170 kW, the required battery power is estimated at 50 kW for the reference configuration.

4.1 Maximum temperature of the fuel cell stack

This paper aims to present a method to identify a configuration that is efficiency and weight-optimised, whilst respecting the limits of the heat management system. Therefore, the first parameter that will be analysed is the maximum fuel cell stack temperature during the flight, as this defines whether the configuration can operate safely with the pre-designed heat management system. The maximum limit for the fuel cell stack temperature in this paper is defined as

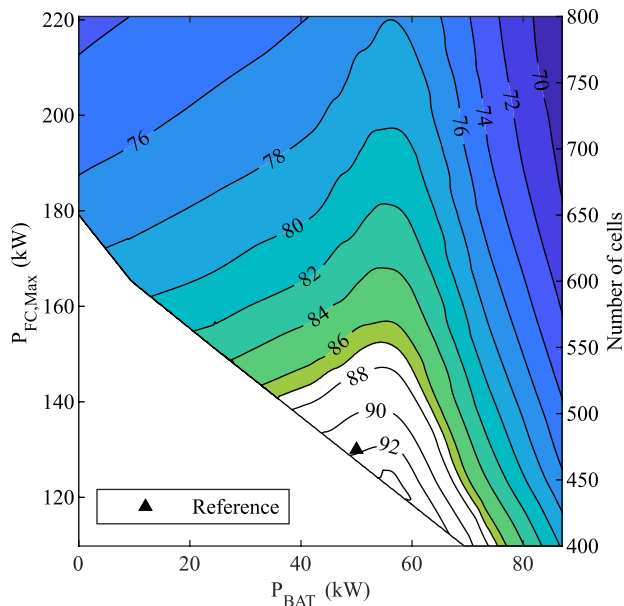


Fig. 9 Maximum temperature of the fuel cell stack during the mission in °C with respect to the maximum fuel cell stack power and the battery power

87 °C [27, 28]. The Fig. 9 shows the maximum fuel cell stack temperature over the whole flight across all configurations. The maximum temperature is presented by isolines with respect to the maximum available power of the fuel cell stack $P_{FC,Max}$ on the y-axis and the battery power P_{BAT} on the x-axis. This format is kept along all analysed parameters. It can be derived, that the maximum temperature of some configurations exceed the limit of 87 °C, therefore these configurations are not to be considered further. These configurations will be highlighted across all following result plots by not applying a colour to these configurations.

The results show, that the reference configuration is one of those, which exceed the maximum fuel cell stack temperature limit. The figure also shows that increasing the battery size causes the maximum fuel cell stack temperature to increase slightly at first, followed by a significant decrease at a certain point. This decrease is related to the decreasing maximum utilised power of the fuel cell stack, which results in a lower generated heat.

Furthermore, it can be seen that the maximum temperature of the fuel cell stack decreases with increasing fuel cell stack size despite constant battery power and thus almost constant utilised power of the fuel cell stack. In addition to the efficiency gain due to oversizing, which leads to lower heat generation, the heat capacity of the fuel cell stack increases. Since the generated heat correlates with the utilised power of the fuel cell stack, the high heat generation rate only applies during the relatively short take-off and climb phase. Therefore, the increased heat capacity due to

the higher fuel cell stack mass mainly drives a reduction of its maximum temperature by increasing its thermal inertia and thus decreasing the change of temperature with respect to time.

4.2 System mass

The aircraft weight mainly defines the power requirement and is therefore one optimisation criteria. It is aimed to minimise the aircraft weight by decreasing the aircraft's component masses. However, this paper assumes a constant mass for all components except for the fuel cell stack and the battery, as it presents a method for the preliminary design. Therefore, a weight optimisation can only be achieved by minimising the system mass M_{sys} , which in this paper is defined as the sum of the fuel cell stack and battery masses for each side of the aircraft. Figure 10 presents the system mass for all analysed configurations, which highlights the improvement of this proposed design method by displaying the deviation of the actual system mass to the system mass of the reference configuration.

It is shown, that the weight-optimised design is reached for a fuel cell-only configuration with no oversizing. For that configuration, a system mass reduction of up to approximately 90.15 kg (63.04%) is determined. The Fig. 10 also shows, that increasing the battery power affects the system mass more significantly than increasing the maximum fuel cell stack power, which is due to the higher power density of fuel cells. For instance, the fuel cell-only configuration with

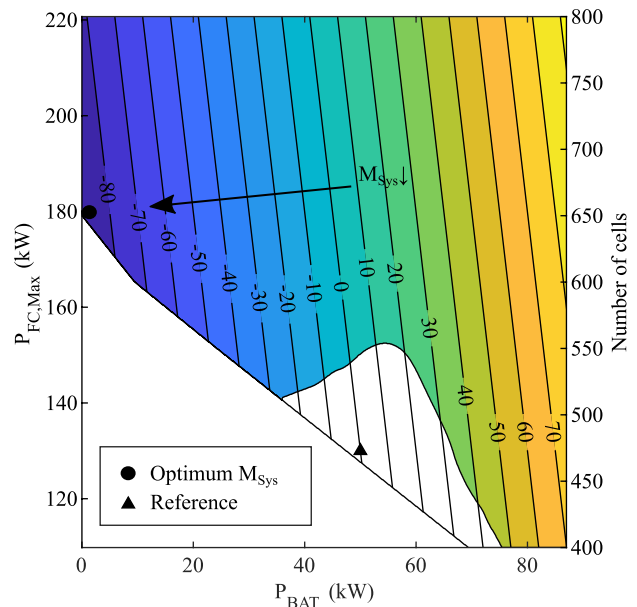


Fig. 10 System mass per side of the aircraft as deviation to the reference configuration in kilogrammes with respect to the maximum fuel cell stack power and the battery power

the highest analysed oversizing would still lead to a system mass reduction of 81.95 kg (57.30%) compared to the reference configuration.

4.3 Overall efficiency

The primary purpose of the propulsion system is to supply the demanded propulsive power by generating the required thrust. Therefore, the output of the propulsion system over the flight can be quantified by integrating the propulsive power over the whole flight. As the battery is charged during the mission, the total input can be quantified by the total mission fuel consumption Δm_{H_2} and the lower heat value of hydrogen H_{u,H_2} . The overall efficiency $\eta_{Overall}$ over the flight can therefore be determined by Eq. (42). The Fig. 11 presents the overall efficiency in percent for the configurations of the performed study.

$$\eta_{Overall} = \frac{\int_{t_{Start}}^{t_{End}} P_{Prop} dt}{\Delta m_{H_2} \cdot H_{u,H_2}} \quad (42)$$

Figure 11 shows, that an increasing battery power at a constant fuel cell stack size generally leads to a slightly decreasing overall efficiency despite allowing the fuel cell stack to operate at a more efficient part load during take-off and climb. This is mainly due by the additional losses that occur during discharging and charging the battery. However, the figure also shows that increasing the maximum fuel cell power improves the overall efficiency significantly. The identified efficiency-optimised configuration is the fuel

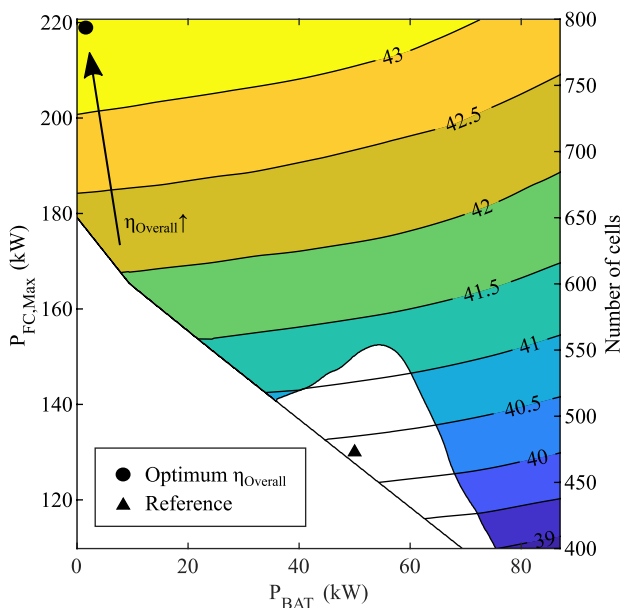


Fig. 11 Overall efficiency over the flight mission in percent with respect to the maximum fuel cell stack power and the battery power

cell-only configuration with the highest analysed oversizing at an overall efficiency of 43.49%. This leads to an efficiency improvement of 3.15%-points as the reference configuration operates at an overall efficiency of 40.34%.

4.4 Mission fuel consumption

The main aim of improving the efficiency is to decrease the mission fuel consumption. However, different configurations lead to different total masses and thus to different required propulsive powers. Hence, a higher efficiency does not automatically lead a lower mission fuel consumption, as an increased mass affects the mission fuel consumption negatively. A weight decrease as well as an efficiency gain are positively affecting the mission fuel consumption. As this paper aims an optimisation in efficiency and weight, the mission fuel burn is used as the objective function combining both criteria into one parameter. Therefore, for this analysis, the mission fuel consumption is separately evaluated and even prioritised. The Fig. 12 presents the mission fuel consumption per side of the aircraft as deviation to the reference configuration.

The reference configuration consumes approximately 9.88 kg of hydrogen per side of the aircraft. Figure 12 shows that an oversized fuel cell-only configuration can lead to a mission fuel consumption decrease of 1.10 kg (11.17%). As shown earlier, the oversized fuel cell-only configuration is the most efficient one. As the system mass and thus the take-off mass does not increase significantly by oversizing

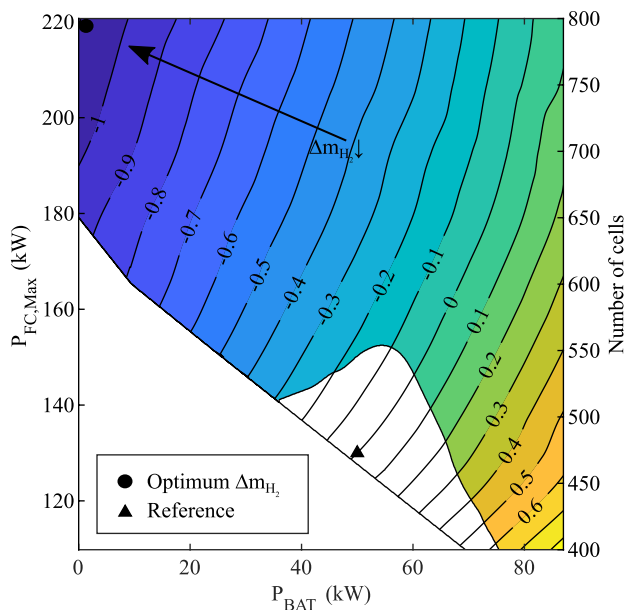


Fig. 12 Mission fuel consumption per side of the aircraft as deviation to the reference configuration in kilograms with respect to the maximum fuel cell stack power and the battery power

the fuel cell stack, the high efficiency by oversizing mainly affects the fuel consumption so that the oversized fuel cell-only configuration is the identified consumption-optimised configuration.

4.5 Summary

The results show, that the optimised weight is reached for the fuel cell-only configuration with no oversizing, which enables a system mass reduction by 90.15 kg (63.04%). However, the efficiency and fuel consumption is optimised for the fuel cell-only configuration with the maximum analysed oversizing. This configuration still yields a reduction of the system mass by 81.95 kg (57.30%), whilst enabling an efficiency gain of 3.15%-points and a fuel consumption decrease of 1.10 kg (11.17%). The efficiency and fuel consumption is prioritised over the system mass. Furthermore, the efficiency and fuel consumption-optimised configuration is only slightly heavier than the weight-optimised configuration. Therefore, as the result of this paper, the fuel cell-only configuration with the highest analysed oversizing is identified as the overall optimised configuration.

5 Conclusion and recommendations

This paper demonstrated a model based preliminary design method for an efficiency and weight-optimised hybrid-electric aircraft. For that, a transient model of an aircraft's propulsion system and heat management system was developed. This model has been used to conduct a parameter study to determine characteristic parameters for different configurations of fuel cell stack and battery sizes. These parameters have been analysed to identify an overall optimised configuration.

The conducted study shows, that the dimensions of the fuel cell stack and the battery have a significant impact on the overall performance of the aircraft's propulsion system. The first main advantage of this design method is to identify all configurations, which respect the limits of the heat management system and can therefore be utilised. The reference configuration for instance was evaluated to exceed the maximum temperature limit and can therefore not be operated without an improvement of the heat management system.

The overall optimised configuration in this paper is identified to be the oversized fuel cell-only configuration with a maximum power of the fuel cell stack of 220 kW. This leads to a system mass decrease of 57.30%, an efficiency gain of 3.15%-points and a reduced fuel consumption by 11.17% when compared to the reference configuration, whilst respecting the limits of the heat management

system. However, for more detailed design phases, it is recommended to analyse the whole "sweet spot area", which for the analysed aircraft and flight mission is identified as all fuel cell-only configurations or configurations with relatively small batteries, given that the characteristic parameter only deviate slightly in this area.

The decreased system mass leads to decreasing requirements on other components such as the structure. Therefore, the more detailed, iterative design phases could potentially show even higher benefits. Furthermore, it was evaluated for the identified "sweet spot area", that the maximum temperature of the fuel cell stack has a big margin to the maximum temperature limit. Therefore, the heat management system could be adjusted by using smaller heat exchanger and air intakes, so that the aircraft weight would decrease further and the drag could decrease, which would even enable a further decreased fuel consumption.

The proposed method for the preliminary design can also be applied in more advanced design phases by increasing the level of detail in the model, which can be achieved by the available data of more advanced design phases. For instance, the component masses of more components such as the compressor, the heat exchanger, structural components etc. would also have to be adjusted for every configuration. Additionally, the level of detail regarding the component behaviour can be increased, as well as adding components to the model which were neglected for the preliminary design, such as the required power of small components like pumps, or the heat management of the batteries and the electric motor. Furthermore, additional limits such as operational limits of components or physical limits regarding the integration can be implemented in order to identify configurations that exceed limits and must therefore be excluded.

Author contributions All authors contributed to the study conception and design. The preparation of the used model, the data collection, as well as the analysis were performed by MA. The first draft of the manuscript was written by MA and NN and all authors commented on previous versions of the manuscript. All authors read and approved the final manuscript.

Funding Open Access funding enabled and organized by Projekt DEAL. The authors would like to acknowledge the European Regional Development Fund (ERDF) and the Business Development Bank of the Federal State of Berlin (IBB) for their financial support of the research project: flying with hydrogen as energy carrier.

Data availability The datasets generated and analysed during the current study are available with restrictions from the corresponding author on reasonable request.

Declarations

Conflict of interest The authors have no competing interests to declare that are relevant to the content of this article.

Open Access This article is licensed under a Creative Commons Attribution 4.0 International License, which permits use, sharing, adaptation, distribution and reproduction in any medium or format, as long as you give appropriate credit to the original author(s) and the source, provide a link to the Creative Commons licence, and indicate if changes were made. The images or other third party material in this article are included in the article's Creative Commons licence, unless indicated otherwise in a credit line to the material. If material is not included in the article's Creative Commons licence and your intended use is not permitted by statutory regulation or exceeds the permitted use, you will need to obtain permission directly from the copyright holder. To view a copy of this licence, visit <http://creativecommons.org/licenses/by/4.0/>.

References

1. Grewe, V., Rao, A.G., Grönstedt, T., Xisto, C., Linke, F., Melkert, J., Middel, J., Ohlenforst, B., Blakey, S., Christie, S., et al.: Evaluating the climate impact of aviation emission scenarios towards the paris agreement including COVID-19 effects. *Nat. Commun.* **12**(1), 1–10 (2021)
2. International Air Transport Association-IATA.: 20 year passenger forecast (2020)
3. Krein, A., Williams, G.: Flightpath 2050: Europe's vision for aeronautics. Innovation for Sustainable Aviation in a Global Environment: Proceedings of the Sixth European Aeronautics Days, vol. 63 (2012). <https://doi.org/10.2777/50266>
4. IATA.: Aircraft technology roadmap to 2050. 05 (2020)
5. Cumpsty, N., Mavis, D., Kirby, M.: Aviation and the environment: outlook, Ch. 1 in ICAO: Environmental Report: Aviation and Environment, p. 2019. Destination Green-The Next Chapter, ICAO (2019)
6. Hoelzen, J., Liu, Y., Bensmann, B., Winnefeld, C., Elham, A., Friedrichs, J., Hanke-Rauschenbach, R.: Conceptual design of operation strategies for hybrid electric aircraft. *Energies* (2018). <https://doi.org/10.3390/en11010217>. (ISSN:1996-1073)
7. Kadyk, T., Schenkendorf, R., Hawner, S., Yildiz, B., Römer, U.: Design of fuel cell systems for aviation: representative mission profiles and sensitivity analyses. *Front. Energy Res.* (2019). <https://doi.org/10.3389/fenrg.2019.00035>
8. Abu Kasim, A.F.B., Chan, M.S.C., Marek, E.J.: Performance and failure analysis of a retrofitted cessna aircraft with a fuel cell power system fuelled with liquid hydrogen. *J. Power Sour.* **521**, 230987 (2022). <https://doi.org/10.1016/j.jpowsour.2022.230987>
9. Kadyk, T., Winnefeld, C., Hanke-Rauschenbach, R., Krewer, U.: Analysis and design of fuel cell systems for aviation. *Energies* **11**(2), 375 (2018). <https://doi.org/10.3390/en11020375>
10. Piper Aircraft, Inc. TYPE-CERTIFICATE DATA SHEET Piper Model PA-46 (2010). https://uploads-ssl.webflow.com/6294ec935022269cdd66e27c/62c6968a1559f5c5fb1c75d8_Europ_ejski%20Certyfikat%20Typu%20-%20M350.pdf
11. Frey, J., Sell, F., Gillespy, R., Pfifer, H.: Aerodynamic design and wind tunnel test of a laminar wing with split flap for a fuel cell powered aircraft. Deutscher Luft- und Raumfahrtkongress 2022 published by Deutsche Gesellschaft für Luft- und Raumfahrt - Lilienthal-Oberth e.V. (2023). <https://doi.org/10.25967/570209>
12. APUS Zero Emission. APUS i-2: The Zero Emission GA Aircraft. https://group.apus-aero.com/wp-content/uploads/2021/09/APUS_i-2_20210901.pdf
13. Bargal, M.H.S., Abdelkareem, M.A.A., Tao, Q., Li, J., Shi, J., Wang, Y.: Liquid cooling techniques in proton exchange membrane fuel cell stacks: a detailed survey. *Alex. Eng. J.* **59**(2), 635–655 (2020). <https://doi.org/10.1016/j.aej.2020.02.005>. (ISSN:1110-0168)
14. Davig, G.H.: Fundamentals of Airplane Flight Mechanics. Springer, Berlin (2007). (ISBN:978-3-540-46571-3)
15. Yechout, T.R., Morris, S.L., Bossert, D.E., Hallgren, W.F.: Introduction to Aircraft Flight Mechanics. American Institute of Aeronautics and Astronautics Inc, Providence (2003). (ISBN:978-1-56347-577-1)
16. Manwell, J.F., McGowan, J.G., Rogers, A.L.: Wind Energy Explained: Theory, Design and Application. Wiley, New York (2010)
17. Aviv, R., Gur, O.: Propeller performance at low advance ratio. *J. Aircr.* **42**, 435–441, 03 (2005). <https://doi.org/10.2514/1.6564>
18. Ansari, S.A., Khalid, M., Kamal, K., Ratlamwala, T.A.H., Husain, G., Alkahtani, M.: Modeling and simulation of a proton exchange membrane fuel cell alongside a waste heat recovery system based on the organic rankine cycle in matlab/simulink environment. *Sustainability* **13**(3), 96 (2021). <https://doi.org/10.3390/su13031218>. (ISSN:2071-1050)
19. Zhu, C., Li, X.: A new one dimensional steady state model for pem fuel cell. *World Electr. Veh. J.* **4**(3), 437–443 (2010). (ISSN:2032-6653)
20. Hoeflinger, J., Hofmann, P.: Air mass flow and pressure optimisation of a pem fuel cell range extender system. *Int. J. Hydrogen Energy* **45**(53), 29246–29258 (2020). <https://doi.org/10.1016/j.ijhydene.2020.07.176>. (ISSN:0360-3199)
21. PowerCellution-PowerCell Sweden AB.: P Stack. <https://www.datocms-assets.com/36080/1636022110-p-stack-v-221.pdf>. Accessed Feb 2023
22. Liso, V., Nielsen, M.P., Kær, S.K., Mortensen, H.H.: Thermal modeling and temperature control of a pem fuel cell system for forklift applications. *Int. J. Hydrogen Energy* **39**(16), 8410–8420 (2014). <https://doi.org/10.1016/j.ijhydene.2014.03.175>. (ISSN:0360-3199)
23. Tschegg, E., Heindl, W., Sigmund, A.: Die Luft und ihre Zusammensetzung, pp. 218–253. Springer, Vienna (1984). https://doi.org/10.1007/978-3-7091-8771-5_18. (ISBN:978-3-7091-8771-5)
24. Lechmann, A.: Modellierung von Wärmeübertragern in den Gaswechselsystemen von Verbrennungsmotoren. Doctoral thesis, Technische Universität Berlin, Fakultät V-Verkehrs- und Maschinensysteme, Berlin (2008). <https://doi.org/10.14279/depositonce-1929>
25. Rubenstein, D., Yin, W., Frame, M.: Mass transport and heat transfer in the microcirculation. In: *Biofluid Mechanics. Biomedical Engineering*, 3rd edn., vol. 96, pp. 331–374. Academic Press (2022). <https://doi.org/10.1016/B978-0-12-818034-1.00008-6> (ISBN:9780128180341)
26. Stieglitz, R., Heinzel, V.: Thermische Solarenergie Grundlagen. Technologie, Anwendungen (2013) 978-3-642-29475-4. 32.23.01; LK 01. Springer, Wiesbaden (2012)
27. Tang, X., Zhang, Y., Sichuan, X.: Temperature sensitivity characteristics of pem fuel cell and output performance improvement based on optimal active temperature control. *Int. J. Heat Mass Transf.* **206**, 123966 (2023). <https://doi.org/10.1016/j.ijheatmasstransfer.2023.123966>. (ISSN:0017-9310)
28. Tawalbeh, M., Alarab, S., Al-Othman, A., Javed, R.M.N.: The operating parameters, structural composition, and fuel sustainability aspects of pem fuel cells: a mini review. *Fuels* **3**(3), 449–474 (2022). <https://doi.org/10.3390/fuels3030028>. (ISSN:2673-3994)

Publisher's Note Springer Nature remains neutral with regard to jurisdictional claims in published maps and institutional affiliations